International Journal of Theoretical Physics, Vol. 33, No. 2, 1994

The Formation and Evolution of Fractal Structure within Chaotic Attractors

Paul Jenkins[1] and Daniel M. Heffernan[1,2]*

Received July 29, 1992

In this paper we examine in detail the formation and evolution of fractal structure in the chaotic attractors of nonlinear dynamical systems. We explicitly obtain the fractal structure of the underlying chaotic attractors of low-dimensional systems and study their evolution as a system parameter is varied. Using periodic enumeration, dimensional, and $f(\alpha)$ spectral techniques, we obtain a detailed characterization of the multifractal structure.

1. INTRODUCTION

One of the major problems in nonlinear dynamics is to quantify a system when it is in a chaotic state (Auerbach *et al.*, 1987; Gunaratne and Procaccia, 1987). In certain cases where there is an underlying strange attractor it is possible to make statistical predictions about the evolution of the system. The evolution dynamics is contained within the structure of the attractor. Hence it is important to understand and quantify the evolution of structure within attractors. In this paper we examine in detail the formation and evolution of fractal structure in the chaotic attractors of simple low-dimensional nonlinear dynamical systems.

The problem is a fundamental and universal one underlying many areas of nonlinear physics (Halsey *et al.*, 1986). Many areas of physics present us with a perplexing variety of complicated fractal objects and strange sets. Notable examples include configurations of Ising spins at critical points (Wilson, 1979), the region of high vorticity in fully developed turbulence (Mandelbrot, 1977; Aref and Siggia, 1981; Procaccia, 1984), percolating clusters and their backbones (de Arcangelis *et al.*, 1985), and

[1]School of Physical Sciences, Dublin City University, Dublin 9, Ireland.
[2]School of Theoretical Physics, Dublin Institute of Advanced Studies, Dublin 4, Ireland.
*Author to which all correspondence should be addressed.

0020-7748/94/0200-0459$07.00/0

diffusion-limited aggregates (Witten and Sander, 1981). The essence of the physics of these problems is to characterize the fractal objects and to describe the events occurring on them (Halsey *et al.*, 1986). This probability measure enables us to treat the problem statistically and to make statistical predictions about the evolution of the system. For example, in dynamical systems theory most physical systems in a (deterministic) chaotic state have an associated strange attractor in phase space and this attractor contains all the information about the behavior of the system. (The relative distribution of points on the attractor is a probability measure for the system in the chaotic state.) In diffusion-limited aggregation single molecules perform a random walk until they become attached on an aggregate producing attractive random fractals reminiscent of certain biological growth patterns or the Lictenberg figures of electrical breakdown on insulating surfaces (Meakin *et al.*, 1985; Stanley and Meaken, 1988; Schroeder, 1991). In this case one is interested in the probability of a random walker landing next to a given site on the aggregate. In percolation one may be interested in the distribution of voltages across the different elements in a random-resistor network (de Arcangelis *et al.*, 1985; Stauffer, 1985). In general one can describe such events if one can determine the structure of the underlining fractal set. However, this task is made difficult by the complicated nature of these sets—they are multifractal (Halsey *et al.*, 1986; Procaccia, 1987).

In this paper we examine in detail the formation and evolution of fractal structure in the chaotic attractors of both linear and nonlinear dynamical systems. We explicitly obtain the fractal structure of the underlying chaotic attractors of low-dimensional systems and study their evolution as a system parameter is varied. It has been shown by Feigenbaum *et al.* (1986, 1989) that from a detailed knowledge of the $f(\alpha)$ spectrum it is possible, in certain cases, to infer the underlining scaling structure of the map. Using periodic enumeration, dimensional, and $f(\alpha)$ spectral techniques, we obtain a detailed characterization of the fractal structure. The paper is divided into sections. In Section 2 we study in detail the formation and evolution of fractal structure on the one-dimensional chaotic attractor of the circle map. In Section 3 Cantor sets are studied in terms of the generalized dimensions and their scaling indices. The results of this section are critical to the study of the formation and evolution of chaotic attractors in higher-dimensional systems. In Sections 4 and 5 we examine the hypothesis that in two-dimensional hyperbolic systems a chaotic attractor is the product of a one-dimensional surface and a one-dimensional Cantor set (Wiggins, 1988). We examine this in detail by obtaining explicitly and studying in detail the fractal structure in two-dimensional linear and nonlinear dynamical systems. In Section 6 the formation of fractal struc-

ture in higher-dimensional dynamical systems is also studied and the Cantor structure of the three-dimensional nonuniform toral map obtained. In three dimensions we find that these Cantor sets can have both a one-dimensional and a two-dimensional structure. Some of the difficulties associated with characterizing higher-dimensional fractal structures are addressed.

2. THE SIMPLE CIRCLE MAP

One of the simplest chaotic one-dimensional maps is the map of the circle which is given by[3]

$$X_{i+1} = AX_i \bmod 1 \tag{1}$$

This is hyperbolic for all values of A excluding $A = \pm 1$. For $A < |1|$ we have periodic solutions, while for $A > |1|$ we have chaotic solutions. This map is not a homeomorphism, since it is not one-to-one and therefore its inverse is not defined. Since this map is defined on a circle $X = 0$ is equivalent to $X = 1$. The Lyapunov exponent λ is given by

$$\lambda = \ln|A| \tag{2}$$

This is positive for $A > 1$. The possibility of divergence and bounded trajectories causes the map to stretch the interval and fold a portion of the

[3]The examples we use in this paper can be motivated as special cases of the periodically kicked rotator (Schuster, 1988):

$$\frac{d^2\phi}{dt^2} + \Gamma\frac{d\phi}{dt} = Kf(\phi)\sum_{n=0}^{\infty}\delta(t - nT), \qquad n \text{ integer}$$

where ϕ is the angular displacement of the rotator, Γ is the damping constant, and we have normalized the moment of inertia to unity. A simple change of variables, $x = \phi$, $y = d\phi/dt$, and $z = t$, enables us to write the forced rotator equation as a set of first-order nonlinear autonomous differential equations:

$$\frac{dx}{dt} = y, \qquad \frac{dy}{dt} = -\Gamma y + Kf(x)\sum_{n=0}^{\infty}\delta(z - nT), \qquad \frac{dz}{dt} = 1$$

The evolution of the rotator between kicks can be obtained by integrating between the limits $(n+1)T - \varepsilon > t > nT - \varepsilon$ to give

$$x_{n+1} = x_n + \frac{1 - e^{-\Gamma T}}{\Gamma}[y_n + Kf(x_n)], \qquad y_{n+1} = e^{-\Gamma T}[y_n + Kf(x_n)]$$

This two-dimensional discrete map is essentially a stroboscopic picture of the time evolution of the 3D differential equations for the rotator. The one- and two-dimensional maps used in this paper are special cases of these equations under different physical conditions. For example, under strong dissipation ($\Gamma \to \infty$) and coupling ($K \to \infty$) such that $\Gamma/K \to 1$ we obtain equation (1) when the applied force is of the form $f(x_n) = (A-1)x_n$.

interval back on itself. The chaotic behavior of this map is examined for $A \in [1, \infty]$. We have computed the correlation dimension D_2 (see below) and have found that $D_2 \approx 1.0$ for all values of $A > 1$.

The nth return map of the circle map is given by $f^n(X) = A^n X$. Thus, X is periodic of period n if and only if $A^n X = X + k$ for some integer k, i.e., if and only if $x = k/(A^n - 1)$, where $0 \leq k < A^n$. Hence the periodic points of period n for the map f of equation (1) are the $(A^n - 1)$th root of unity. It follows that periodic points are dense on the unit interval (Devaney, 1989). It is important to note that for A an integer the orbits are distributed uniformly along the unit interval.

2.1. The Probability Density on the Circle Map Attractor

The probability density has been computed numerically for $A = 1.1$, 2.0, and 2.5 and is shown in Fig. 1. For $A = 2.0$ the probability density is uniform. In general the probability density is uniform when A is an integer. This uniform distribution can be explained in terms of the periodic orbits. For A an integer there is a uniform distribution of periodic orbits along the unit interval. Hence we would expect a uniform probability. As A tends

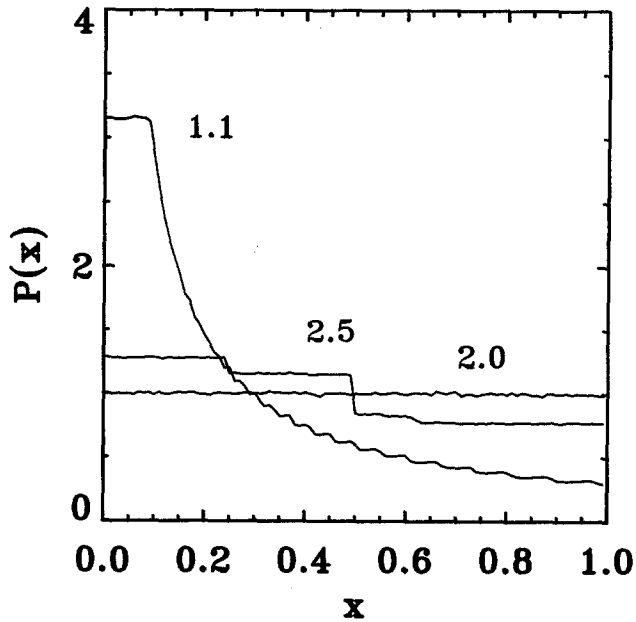

Fig. 1. Probability density $P(X)$ vs. X for the circle map. Three values of A are shown, 1.1, 2.0, and 2.5.

toward infinity we also get a uniform probability density because the time series is completely random. The entropy is $\ln A$. Small entropy corresponds to a deterministic system and large entropy corresponds to a completely random system. For nonintegral A, the peaks in the probability distribution can be related to a high concentration of periodic orbits at that position along the interval.

2.2. The $f(\alpha)$ Spectrum of the Circle Map

Using the probability density that we calculated in the previous section, we can calculate the $f(\alpha)$ spectrum and the corresponding D_q spectrum of dimensions for the circle map (Duong-van, 1987). For $A = 2.5$ the probability density can be approximated by

$$p(X) = \begin{cases} 1.28 & 0.00 < X \leq 0.25 \\ 1.15 & 0.25 < X \leq 0.50 \\ 0.84 & 0.50 < X \leq 0.60 \\ 0.77 & 0.60 < X \leq 1.00 \end{cases} \tag{3}$$

We start with this probability and subdivide the interval [0, 1] into n segments of size l_i, each with a constant probability $P_i = a$, where a is now the area chosen in the following manner:

$$a = \int_{X_{i-1}}^{X_i} p(X)\, dX \qquad \text{with} \quad p(X) \text{ normalized to 1} \tag{4}$$

Given a chosen a, X_i can be calculated. The segment $l_i = X_i - X_{i-1}$ with the corresponding $P_i = a$ can now be used in the relation (Duong-van, 1987)

$$\sum_{i=1}^{1/a} \frac{P_i^q}{l_i^{(q-1)Dq}} = 1 \tag{5}$$

to solve for D_q. The numerical results are presented in Fig. 2, where we show D_q as a function q. Using equation (5), we can compute the corresponding $f(\alpha)$ spectrum and this is shown in Fig. 3. For $q = 0$ we simply obtain $f = D_0 = 1.0$, where D_0 is the Hausdorff dimension of the set. The Hausdorff dimension of a one-dimensional unstable manifold is always $D_0 = 1.0$. Both $f(\alpha)$ and D_q have no essential difference in describing the global character, except for the Legendre transform with which they are linked:

$$\alpha = \frac{d}{dq}[(q-1)D_q], \qquad f(\alpha) = q\alpha - (q-1)D_q \tag{6}$$

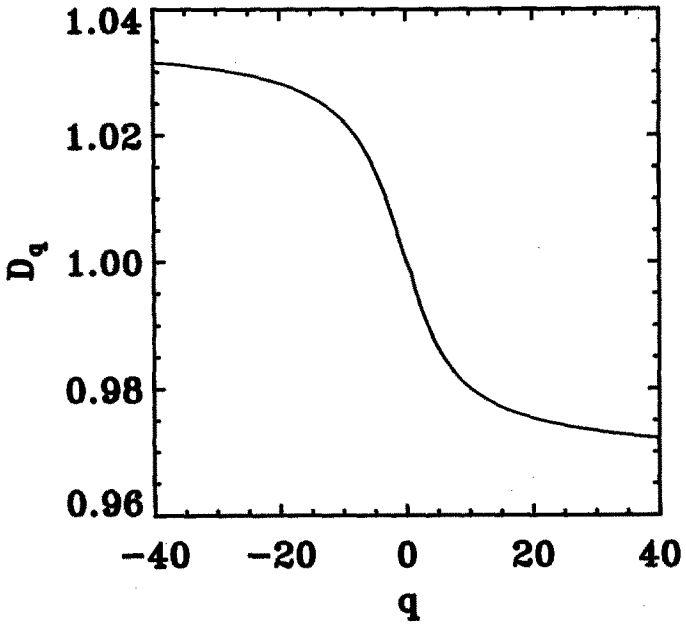

Fig. 2. D_q vs. q for the circle map with $A = 2.5$.

We have also evaluated the spectrum of generalized dimensions and the $f(\alpha)$ spectrum from the generalized correlation function (Hentschel and Procaccia, 1983) and have found the result to be in excellent agreement with the analysis above for positive q. For negative q, deviations of a few percent are found for the approximate probability distribution [equation (3)] used above.

A similar calculation for $A = 2$ gives $D_q = 1$ $\forall q \in [-\infty, \infty]$. For this value of $A = 2$ we have an example of a uniform hyperbolic attractor. $A = 1.1$ and 2.5 are examples of nonuniform hyperbolic attractors. Note that the probability density is related to the concentration of period orbits at a particular point along the interval.

3. CANTOR SETS

A large number of strange attractors have a Cantor set underlining their structure. In this section we examine Cantor sets from the point of view of their spectrum of generalized dimensions and their spectrum of Lipschitz–Hölder scaling indices. Cantor sets are of fundamental importance to the understanding of chaos, as the chaotic attractors of many

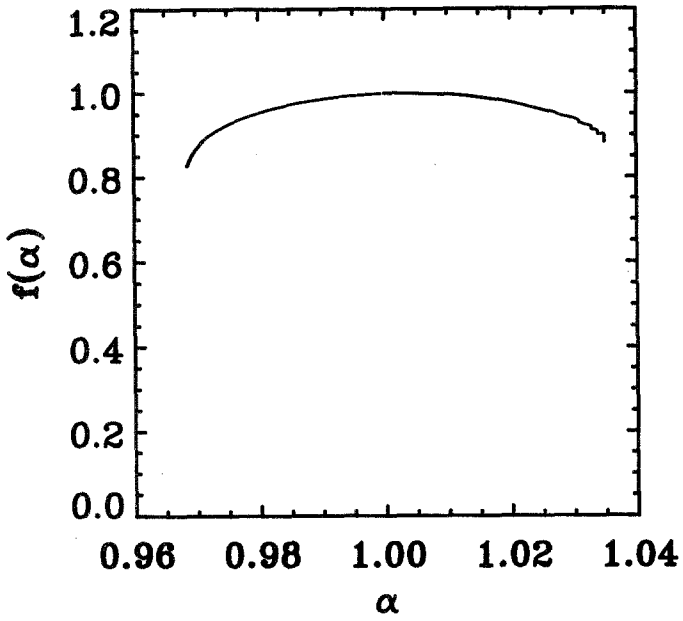

Fig. 3. The function $f(\alpha)$ vs. α for the circle map evaluated at $A = 2.5$.

important dynamical systems have such structure [see Tél (1988) for an excellent review of the whole area]. We will now review that area of Cantor theory that is pertinent to our analysis.

If a measure is constructed from an exact recursive rule, one can easily determine the D_q and $f(\alpha)$ spectra. For example, suppose that the measure is generated by the following process. Start with the original region which has a length one. Divide the region into pieces S_i, $i = 1, 2, \ldots, N$, with probabilities P_i and lengths l_i. At the first stage we can construct a partition function (Halsey *et al.*, 1986)

$$\Gamma_1(\tau, q) = \sum_{i=1}^{N} \frac{P_i^q}{l_i^\tau} \tag{7}$$

At the next stage each piece of the set is further divided into N pieces, each with a probability reduced by a factor P_i and the size by a factor l_i. At this stage the partition function is given by

$$\Gamma_2(\tau, q) = \Gamma_1^2(\tau, q) \tag{8}$$

Now it can be seen that the first partition function will generate all the others, that is, $\Gamma_n = \Gamma_1^n$. For this reason Γ_1 is called a generator for the set.

3.1. The Uniform Cantor Set

A simple example of a uniform Cantor set is the middle third Cantor set. The interval [0, 1] is divided as follows. Start with the unit interval but remove the open middle third, i.e., the interval [1/3, 2/3]. Each of the remaining intervals receives the same probability measure $P = 1/2$. This procedure is continued indefinitely. Note that 2^n open intervals are removed at the nth stage of this process. Thus for this measure we require that $2[(1/2)^q/(1/3)^\tau] = 1$, which yields $\tau = (q-1)\ln 2/\ln 3$ and $D_q = \ln 2/\ln 3$ (Tél, 1988). This Cantor set has a point $f(\alpha)$ spectrum, $\alpha = f = D_q$. This uniform Cantor set is an example of a simple fractal. Intuitively, a fractal is a set which is self-similar under magnification. By varying the interval size l_i, we can vary the dimension $D_q = \ln P/\ln l$ of this Cantor set. For $D_q = 1$ we no longer have the self-similar structure, but a line segment of uniform probability. Although this example was trivial, we shall see in Section 4 the importance of uniform Cantor sets when we examine two-dimensional chaotic attractors. A more general example of a Cantor set is the two-scale Cantor set.

3.2. Two-Scale Recursive Sets

Suppose that the measure is generated by the following process. Start with original segment with measure one and size one. Divide the region into pieces of two sizes and probabilities. Let n_1 denote the number of pieces of length l_1 and n_2 the number of length l_2. Further, let the respective probabilities be P_1 and P_2. The probabilities are normalized such that $n_1 P_1 + n_2 P_2 = 1$. The generator is given by

$$\Gamma^n(\tau, q) = \left(n_1 \frac{P_1^q}{l_1^\tau} + n_2 \frac{P_2^q}{l_2^\tau} \right)^n \tag{9}$$

$\tau(q)$ is defined through $\Gamma(\tau, q) = 1$. A special case to which we refer extensively in this paper is the two-scale Cantor set, where $n_1 = n_2 = 1$. This is illustrated in Fig. 4. For $l_1 = l_2$ and $P_1 = P_2$ we obtain the uniform Cantor set discussed in Section 3.1. Using the binomial expansion, we can write equation (9) as

$$\Gamma(q, \tau) = \sum_{m=0}^{n} \binom{n}{m} n_1^m n_2^{(n-m)} P_1^{mq} P_2^{(n-m)q} (l_1^m l_2^{(n-m)})^{-\tau(q)} \tag{10}$$

Using the analytic methods of Halsey *et al.*, we obtain the following analytic expression for the $f(\alpha)$ spectrum (Halsey *et al.*, 1986):

$$\tau = \frac{\ln(n/m - 1) + q \ln(P_1/P_2)}{\ln(l_1/l_2)} \tag{11}$$

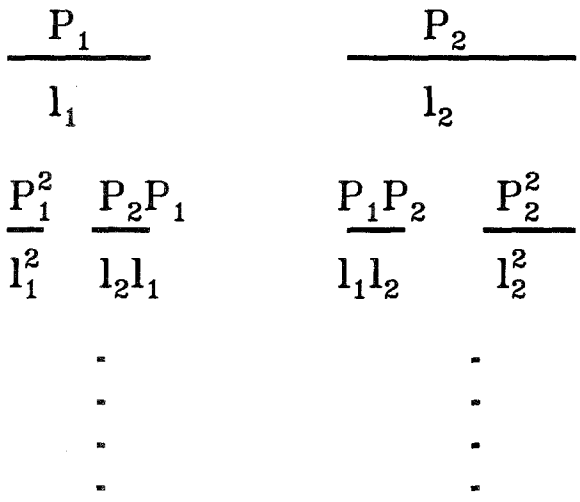

Fig. 4. The two-scale Cantor set.

and

$$f = \frac{(n/m - 1)\ln(n/m - 1) - (n/m)\ln(n/m)}{\ln(l_1) - (n/m - 1)\ln(l_2)} \tag{12}$$

The Lipschitz–Hölder exponents determining the singularity in the measure, α, are determined by (Halsey *et al.*, 1986)

$$P_1^m P_2^{(n-m)} = (l_1^m l_2^{(n-m)})^\alpha \tag{13}$$

or, equivalently,

$$\alpha = \frac{\ln(P_1) + (n/m - 1)\ln(P_2)}{\ln(l_1) - (n/m - 1)\ln(l_2)} \tag{14}$$

We have numerically obtained $D_q\,[=\tau(q)/(q-1)]$ as a function of q by solving equation (9) and the result is shown in Fig. 5. In Fig. 5 we show D_q as a function of q for $P_1 = 0.6$, $P_2 = 0.4$, $l_2 = 0.1$, and $l_1 = 0.1$, 0.3, and 0.7, respectively. The corresponding $f(\alpha)$ spectra are shown in Fig. 6. For any chosen q, the measure scales as $\alpha(q)$ on a set of segments which converge to a set of dimension $f(q)$. As q is varied, different regions of the set determine

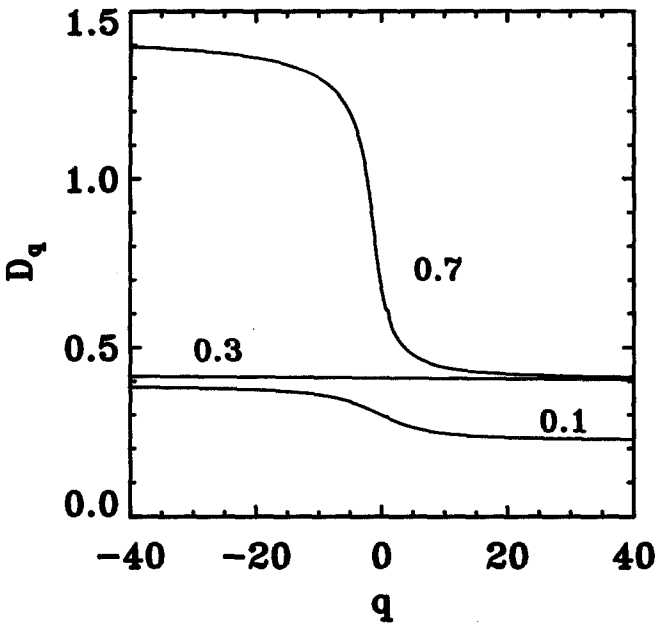

Fig. 5. D_q plotted against q for the two-scale Cantor set, with probabilities $P_1 = 0.6$ and $P_2 = 0.4$ and length scaling $l_2 = 0.1$. Three different values of the length scale l_1 are used, 0.1, 0.3, and 0.7.

D_q. The extreme α values are

$$D_{-\infty} = \alpha_{\max} = \ln P_2 / \ln l_2 \qquad \text{and} \qquad D_{\infty} = \alpha_{\min} = \ln P_1 / \ln l_1 \tag{15}$$

For $q = 0$ we simply obtain $f = D_0$, where D_0 is the Hausdorff dimension of the set. This is the maximum of the graph of $f(\alpha)$.

Some of the most interesting problems lie on supports of continuous measure, including the circle map strange attractor and ordinary differential equations. Supports of continuous measure have a Hausdorff dimension $D_0 = 1$. A unit interval is divided into three segments such that $l_1 + l_2 + l_2 = 1$, with probability distributions P_1, P_2, and P_2, respectively (Tél, 1988).

To fix our ideas, consider the following example: $l_1 = 0.2$ and $l_2 = 0.4$, with $P_1 = 0.1$, $P_2 = 0.45$. Note that $P_2/l_2 > P_1/l_1$ and $l_2 > l_1$. Although the measure on the line segment is rearranged at each step of the recursive process, the support for the measure remains at each step the original line segment. Thus, as we would expect, $D_0 = 1$. The $f(\alpha)$ spectrum for these parameters is shown in Fig. 7. The densest regions on the line segment

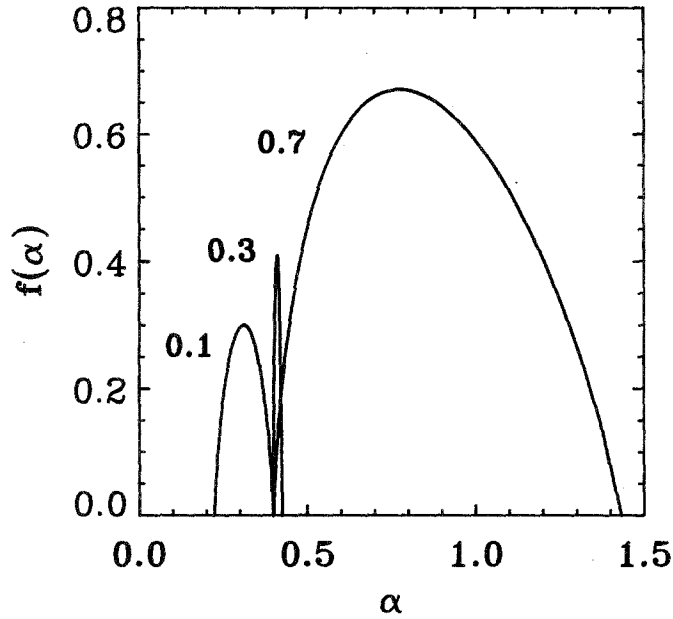

Fig. 6. A plot of $f(\alpha)$ vs α for the two-scale Cantor set, with probabilities $P_1 = 0.6$ and $P_2 = 0.4$ and length scaling $l_2 = 0.1$. Three different values of the length scale l_1 are used, 0.1, 0.3, and 0.7.

contract not to one point, but to a set of points of finite dimension. The lowest value of α and D_∞ is $D_\infty = \alpha = \log(0.45)/\log(0.4) = 0.87$, with a corresponding nonzero value of $f = 0.756$. Note that there is always only one segment at the lowest values of the density, so that we still expect $D_{-\infty}$ to correspond to a value of $f = 0$. It is also possible to construct a Cantor set for which the most rarefied region corresponds to a set of finite dimension.

4. THE BAKER'S MAP

In Sections 4 and 5 we explore chaos in two- and higher-dimensional discrete systems. The hypothesis (Wiggins, 1988, and references therein) that in two-dimensional hyperbolic systems a chaotic attractor is the product of a one-dimensional surface and a one-dimensional Cantor set is investigated. We will examine this in detail by obtaining and studying the formation and evolution of fractal structure in two-dimensional dynamical systems. One of the simplest dynamical systems is the baker's map (Schus-

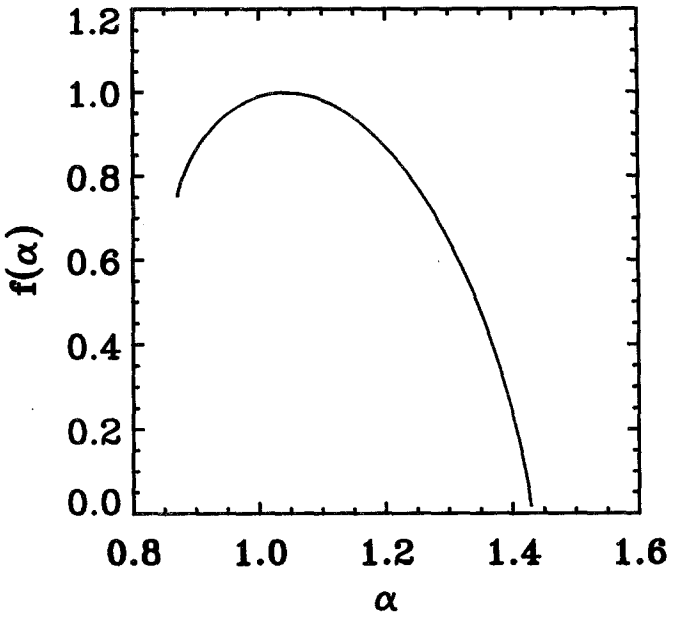

Fig. 7. The function $f(\alpha)$ for the three-scale Cantor set, with probabilities $P_1 = 0.1$ and $P_2 = P_3 = 0.45$ and length scalings $l_1 = 0.1$ and $l_2 = l_3 = 0.4$. Note that D_∞ corresponds to a nonzero value of $f = 0.756\ldots$.

ter, 1988). The baker's map is fundamental to statistical physics (Arnold and Avez, 1968), and both classical and quantum chaos (Balazs and Voros, 1989). The generalized baker's map is defined (Balatoni and Renji, 1956) by the recursion relations on the unit square

$$\begin{pmatrix} X_{i+1} \\ Y_{i+1} \end{pmatrix} = \begin{cases} \begin{pmatrix} R_1 X_i \\ Y_i/S \end{pmatrix}, & 0 \le Y \le S \\ \begin{pmatrix} 1/2 + R_2 X_i \\ (Y_i - S)/(1-S) \end{pmatrix}, & S < Y \le 1 \end{cases} \tag{16}$$

with R_1, $R_2 < 1/2$, $S < 1$. This is a uniformly hyperbolic system. By uniform we mean the probability density is constant along the unstable manifold, that is, the probability density does not depend on the parameters R_1, R_2, and S. Because it is a hyperbolic map, stable and unstable directions are defined everywhere. The strange attractor is the closure of the unstable manifolds of periodic points. The attractor lies along the unstable manifold in the Y direction. This manifold consists of an infinite

number of line segments. The manifold originates from the periodic orbits. The Cantor set is in the X direction.

4.1. The Relationship of the Baker's Map to Cantor Sets

Using symbolic dynamics with the partition $\chi(X, Y) = 1$ for $Y > S$ and $\chi(X, Y) = 0$ for $Y < S$, we find that every sequence of 1's and 0's is allowed and that there are 2^n orbits belonging to an unstable orbit of period n (Procaccia, 1987). The eigenvalues of the n-cycle depend only on the number of 1's and 0's in the sequence. Denoting the number of 0's by m, we find that the Lyapunov scaling factors at the nth iteration are given by (Procaccia, 1987; Auerbach *et al.*, 1988; Grebogi *et al.*, 1988)

$$\varepsilon_1^{(n)} = S^{-m}(1-S)^{-(n-m)}, \qquad \varepsilon_2^{(n)} = R_1^m R_2^{(n-m)} \tag{17}$$

The partition function is related to the stability of the unstable orbits by (Grebogi *et al.*, 1988)

$$\Gamma(q, D_q) = \sum \varepsilon_1^{-q} \varepsilon_2^{-(D_q - 1)(q-1)} \tag{18}$$

where the sum is over all unstable orbits of period n. Equation (18) can be used when the probability density is uniform along the unstable manifold. Inserting equation (17) into equation (18), we obtain

$$\Gamma(q, D_q) = \sum_{m=0}^{n} N_{nm} S^{mq}(1-S)^{(n-m)q}(R_1^m R_2^{(n-m)})^{-(D_q-1)(q-1)} \tag{19}$$

where N_{nm} is the number of fixed points of the n-times-iterated map which belong to periodic orbit with m 0's in its sequence. N_{nm} is the number of ways of arranging m zeros and $n - m$ ones,

$$N_{nm} = \binom{n}{m} \tag{20}$$

Apart from the power $(D_q - 1)$, equation (19) is equivalent to equation (10), which was obtained for the two-scale Cantor set. The parameters S, $(1-S)$, R_1, and R_2 are related to P_1, P_2, l_1, and l_2, respectively, of the two-scale Cantor set, namely, $S = P_1$, $1 - S = P_2$, $R_1 = l_1$, and $R_2 = l_2$ (Procaccia, 1987). Thus for this baker's map the Cantor structure of the attractor can be explicitly obtained.

For parameters $S = 1/2$ and $R = R_1 = R_2$ the baker's map is equivalent to the uniform Cantor set we examined in Section 3.1 with the point $f(\alpha)$ spectrum. Attractors belonging to this map are shown in Figs. 8a–8d for $R = 0.1$, 0.3, 0.4, and 0.5, respectively. The dimensions D_q are 1.3, 1.58, 1.75, and 2.0, respectively. The first three are examples of strange attractors

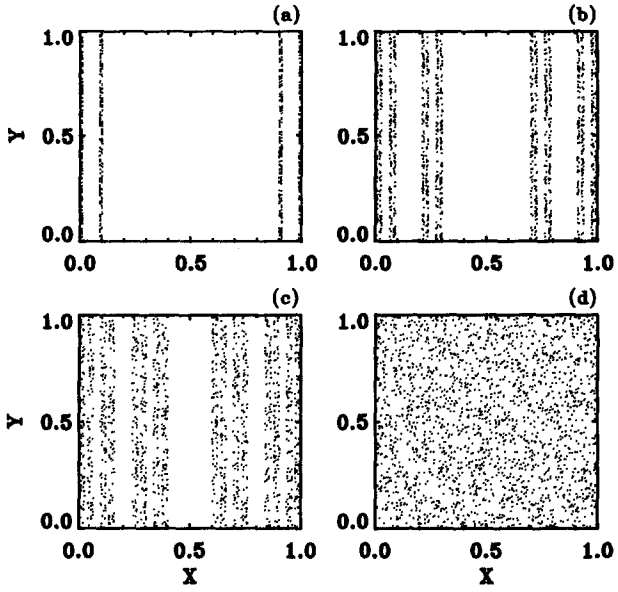

Fig. 8. Attractors for the baker's map with $T = 2.0$ and (a) $R = 0.1$, (b) $R = 0.3$, (c) $R = 0.4$, and (d) $R = 0.5$. The structure of these attractors is related to the middle third Cantor set. They are self-similar under all scales of magnification.

and are self-similar under all scales of magnification. As the parameter R is increased, the unstable orbits redistribute, causing changes in the structure of the attractor. Since the dimension D_q in the Y direction is constant, the increase in dimension and the corresponding change in structure are related to changes in the Cantor set. We have established in Section 2 that the Hausdorff dimension D_0 along the unstable manifold is one. Therefore the increase in Hausdorff dimension for a two-dimensional system is due to changes in the dimension of the Cantor set.

In this case we can also obtain the generalized entropies and the fluctuations around the K entropy as follows (Eckman and Procaccia, 1986);

$$\sum_{m=0}^{n} \binom{n}{m} S^{mq}(1-S)^{(n-m)q} = \exp[-n\tau(q)] \tag{21}$$

where $\tau(q) = (q-1)K_q = \lambda q - g(\lambda)$. Here K_q is the generalized Kolmogorov entropy and $g(\lambda)$ the fluctuation spectrum (Schuster, 1988). In the limit $n \to \infty$ the largest term in the sum of the right-hand side of equation (21)

should dominate. To find this term we note that the maximum occurs when

$$\frac{\delta}{\delta m} \ln\binom{n}{m} S^{mq}(1-S)^{(n-m)q} = 0 \tag{22}$$

Using Stirling's approximation, we find

$$q = \frac{\ln(n/m - 1)}{\ln(1-S) - \ln(S)} \tag{23}$$

The fluctuation spectrum is determined by

$$\binom{n}{m} = \exp[ng(\lambda)] \tag{24}$$

i.e., on applying Stirling's approximation,

$$g = \ln(n/m) - (1 - m/n)\ln(n/m - 1) \tag{25}$$

The exponent determining the singularity in the measure, λ, is determined by

$$S^{mq}(1-S)^{(n-m)q} = \exp(-n\lambda q) \tag{26}$$

or

$$\lambda = \frac{m\ln(S) + (n-m)\ln(1-S)}{-n} \tag{27}$$

Thus, for any chosen q, the measure scales as $\lambda(q)$ on a set of segments which converge to a set of entropies $g(q)$. As q is varied, different regions of the set determine K_q. In Fig. 9 we show the $g(\lambda)$ spectrum of the baker's map for the parameters $S = 0.4$, 0.3, and 0.2.

4.2. The Symbolic Dynamics of the Baker's Map

Consider the baker's map in the following form (Graham and Hamm, 1991):

$$\binom{X_{i+1}}{Y_{i+1}} = \begin{cases} \binom{R_1 X_i}{TY_i}, & 0 \le Y \le 1/2 \\ \binom{1 - R_2(1-X_i)}{1 - T(1-Y_i)}, & 1/2 < Y \le 1 \end{cases} \tag{28}$$

with R_1 and $R_2 < 1$. Strange attractors are obtained for $1 < T \le 2$ and strange repellers for $T > 2$. In this form the number of periodic orbits of period n is T^n, independent of the parameter R. The number of periodic points belonging to periodic orbits of length n in the map is presented in

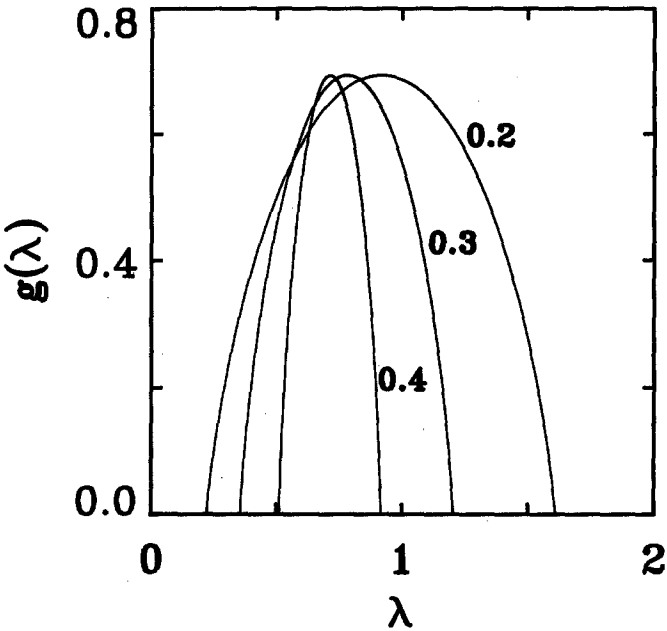

Fig. 9. The generalized Kolmogorov entropy fluctuation spectrum $g(\lambda)$ vs. λ for three different values of S, 0.2, 0.3, and 0.4. The range of λ extends, for fixed S, from $-\ln(S)$ to $-\ln(1-S)$.

Table I for four values of T, namely $T = 1.2$, 1.4, 1.8, and 2.0. The smaller the value of T, the slower the convergence to the theoretical value T^n.

Each orbit has a unique binary label and the periodic points lie on a binary tree. Numerically we have determined the periodic points for a period up to 54. The partition is at $Y = 0.5$. The partition is defined by a 0 for a Y less than 0.5 and a 1 for Y greater than 0.5. Any orbit on the attractor can be represented by a pair of numbers γ and δ called the symbolic plane (Cvitanovic *et al.*, 1988). δ and γ are defined by

$$\delta = 1 - \sum_{k=1}^{\infty} d_k 2^{-k}, \qquad \text{where} \quad d_k = \sum_{i=1}^{k} (1 - a_{-i}) \bmod 2 \tag{29}$$

$$\gamma = \sum_{k=1}^{\infty} c_k 2^{-k}, \qquad \text{where} \quad c_k = \sum_{i=1}^{k} a_i \bmod 2 \tag{30}$$

The symbolic plane for $T = 1.2$ is shown in Fig. 10a. The points belonging to periodic orbits of length 40 are plotted. The allowed orbits are represented by blocks in the symbolic plane. Only even values of period n are

Table I. The Number of Periodic Points Belonging to Periodic Orbits of Length n in the Baker's Map[a]

T	Period	T^n	N_n	$K_0^{(n)}$
1.2	24	80	268	0.2329
	28	164	450	0.2182
	32	341	1020	0.2165
				$\overline{0.1823}$
1.48	24	12197	12654	0.3935
	26	26718	27510	0.3932
	27	39542	38314	0.3913
				$\overline{0.3920}$
1.8	12	1156	1152	0.5874
	14	3748	3782	0.5884
	18	39346	39314	0.5877
				$\overline{0.5878}$
2.0	13	8192	8192	0.6931
	14	16384	16384	0.6931
	15	32768	32768	0.6931
				$\overline{0.6931}$

[a]The third column is the theoretical value expected from the universal grammar. The fourth column is the number of orbits obtained. See text for explanation of the difference. The last column is the nth-order approximant of the topological entropy.

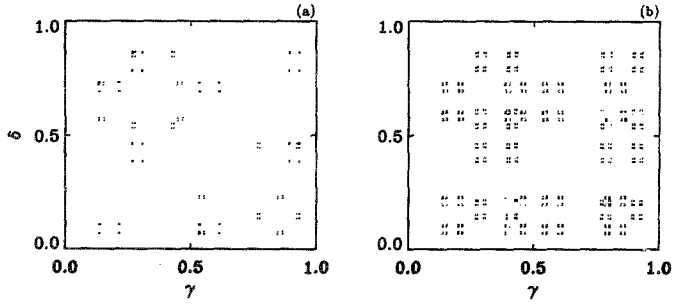

Fig. 10. The symbolic plane of the baker's map for (a) $T = 1.2$ and (b) $T = 1.4$.

allowed. No itinerary containing any of the blocks 000 or 111 is allowed. In contrast, the symbolic plane for $T = 1.4$ is shown in Fig. 10b. With increasing T the orbits are pruned in a systematic way. In Table II we list the low-order forbidden orbits for $T = 1.2$ and 1.4, respectively.

In Figs. 11a and 11b we show the strange attractor for $R = 0.6$ and $T = 1.2$ and $T = 1.4$. It is apparent from these figures that as the parameter

Table II. Forbidden Words in the Symbolic Plane of the Baker's Map for $T = 1.2$ and $T = 1.4$

$T = 1.2$		$T = 1.4$	
Period	Forbidden word	Period	Forbidden word
3	000	3	000
3	111	3	111
6	100100	6	100100
6	110110	6	110110
7	1010100	9	110010100
7	1101010	10	1010010100
9	110010100	10	1101011010
10	1010010100	12	101010101100
10	1101011010	12	110101010100
10	1011001100	14	10101001010100
12	110100110100	14	11010101101010
12	101100101100		

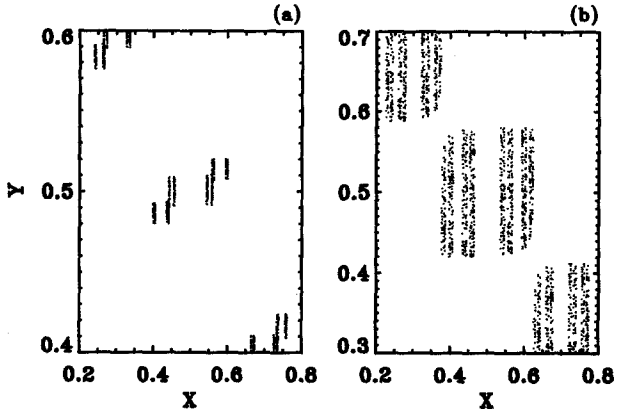

Fig. 11. Attractors for the baker's map with $R = 0.6$ and (a) $T = 1.2$ and (b) $T = 1.4$.

T is decreased, the loss of structure is related to the pruning of the periodic orbits. The attractor has a uniform probability in the Y direction and in the X direction the stable manifold lies on a pruned Cantor set.

4.3. The $f(\alpha)$ Spectrum of Pruned Cantor Sets

We have obtained the $f(\alpha)$ spectrum for $R_1 = 0.2$ and $R_2 = 0.3$ and for three values of T, namely, $T = 1.48$, 1.8, and 2.0. We can use the following

equation to obtain the $f(\alpha)$ spectrum:

$$\Gamma(q, \tau) = \sum_{m=0}^{n} N_{nm} T^{-nq} (R_1^m R_2^{(n-m)})^{-\tau(q)} \tag{31}$$

where the sum includes only allowed orbits. The allowed orbits are specified by N_{nm}. For $T < 2$ the total number of orbits N_{nm} is determined using the procedure discussed in Auerbach *et al.* (1988). For $T = 1.48$ and $n = 27$ the following coefficients were obtained: $N_{27,12} = 306$, $N_{27,13} = 19062$, $N_{27,14} = 19062$, $N_{27,15} = 306$. For $m < 12$ and $15 < m \leq 27$ the coefficients are zero. After calculating N_{nm} for a chosen n, $\tau(q)$ is calculated from equation (31) and then the $f(\alpha)$ spectrum is obtained via the Legendre transform, equation (6). The calculated $f(\alpha)$ spectrum is shown in Fig. 12. The calculations converge well; in fact, similar results were obtained for orbits of period less than 27. For $T = 1.8$, orbits of period 18 give the following nonzero coefficients: $N_{18,6} = 54$, $N_{18,7} = 1980$, $N_{18,8} = 9720$, $N_{18,9} = 15806$, $N_{18,10} = 9720$, $N_{18,11} = 1980$, $N_{18,12} = 54$. For $m < 6$ and $12 < m \leq 18$ the coefficients are zero. The resulting $f(\alpha)$ spectrum is also shown in Fig. 12. For $T \leq 1.4$ all allowed orbits contribute one α value to the spectrum, which results in a point spectrum. For $T = 1.48$ and 1.8,

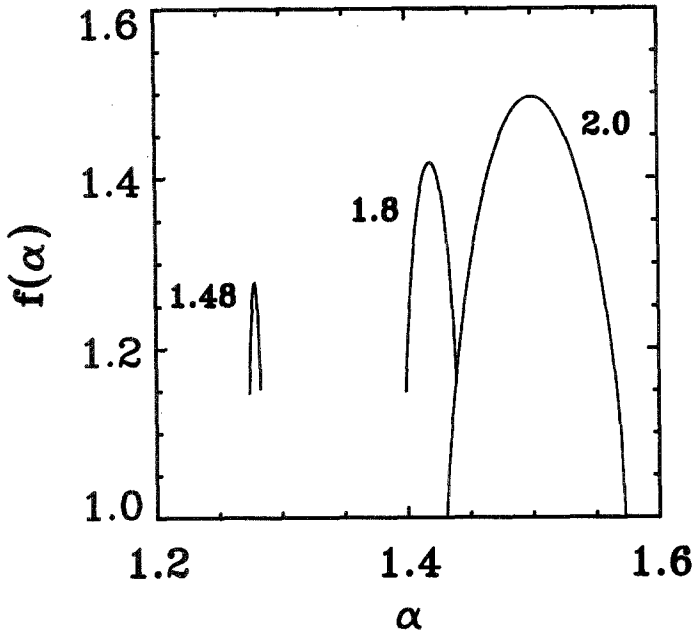

Fig. 12. The $f(\alpha)$ spectrum of the baker's map for the parameters $T = 1.48$, $T = 1.8$, and $T = 2.0$.

because of the nature of the pruning, $\alpha_{\max}$ and $\alpha_{\min}$ correspond to a nonzero value of f. The continuous line for $T = 2$ corresponds to the $f(\alpha)$ spectrum for the two-scale Cantor set of equation (9).

5. THE TWO-DIMENSIONAL HYPERBOLIC TORAL MAP

In this section, we introduce a completely different class of dynamical system, the hyperbolic toral map. One difference between these maps and those that are discussed elsewhere in this paper is that these maps are defined on a torus rather than on Euclidean space. Even though the maps are induced by linear maps on Euclidean space, the maps on the tori have extremely rich dynamical structure. Previous studies have concentrated on the case where the coefficients are integers (Isola, 1990; Vivaldi, 1987; Eckmann and Ruelle, 1985; Arnold and Avez, 1968, and references therein).

Consider the hyperbolic toral map $L_A: T \to T$, where

$$A = \begin{pmatrix} a & b \\ c & d \end{pmatrix} \tag{32}$$

with a, b, c, and $d \in \mathbb{R}$. L_A is clearly differentiable, since its Jacobian matrix is simply the matrix A, with $\det(A) = ad - bc$. The eigenvalues are given by

$$\varepsilon_{\pm} = \frac{1}{2}\{(a+d) \pm [(a+d)^2 + 4bc - 4ad]^{1/2}\} \tag{33}$$

with eigenvectors of slope $c/(\varepsilon_{\pm} - d)$. Only real eigenvalues will be considered. When both of the eigenvalues satisfy $|\varepsilon| < 1$ we have periodic solutions. The transition from periodic to chaotic behavior corresponds to one of the eigenvalues crossing the unit circle. A periodic orbit of period n has stability ε^n. We will now examine the mechanism for chaos in this system.

5.1. The Development and Evolution of the Strange Attractor of the 2D Toral Map

One of the eigenvalues ε_s satisfies $|\varepsilon_s| < 1$ and the other ε_u satisfies $|\varepsilon_u| > 1$. The stable and unstable subspaces W^s and W^u are lines parallel to the eigenvectors corresponding to the eigenvalues ε_s and ε_u. The stable and unstable subspaces W^s and W^u are dense in T for each $(x, y) \in T$. Previous studies of this map have only concentrated on the integer case with determinant one. It is commonly stated that the reason W^s and W^u are dense is because they have irrational slope and hence these curves wind densely around the torus (Devaney, 1989).

In the dissipative case, where the determinant is <1, there is the possibility of chaos in a toral map with rational slope. For example, for the parameters $a=1$, $b=7/5$, $c=2/5$, and $d=0$ the unstable subspace has slope 2/7. Therefore, W^s and W^u do not wind densely around the torus, but we still have chaos, since $|\varepsilon_u|>1$. The subspaces are dense in this case because the stable and unstable manifolds emanate from the infinite number of periodic orbits. Each orbit of period n has its own subspaces W^s and W^u, which may be degenerate with other orbits of different period. The manifold for this system is not continuous, but consists of an infinite number of line segments.

We will now examine the evolution of structure in the attractor as a parameter is varied. Consider the map defined by the parameters arbitrarily chosen to be $A=1.0$, $B=7/5$, $D=0.0$, and C in the range $[0, 1/B]$. As shown in Fig. 13, by varying C in this range, the Lyapunov dimension D_L of the attractor changes from one to two. Shown in Figs. 14a–14d is the attractor for $C=1/5$, 2/5, 1/2, and $1/B=5/7$, respectively. The Lyapunov dimensions of these attractors are 1.14, 1.37, 1.52, and 2.0, respectively. The dimension of each orbit is equivalent to the global dimension of the attractor. We have computed the spectrum of generalized dimensions D_q for q positive and have found that they are constant and equal to D_L. It is

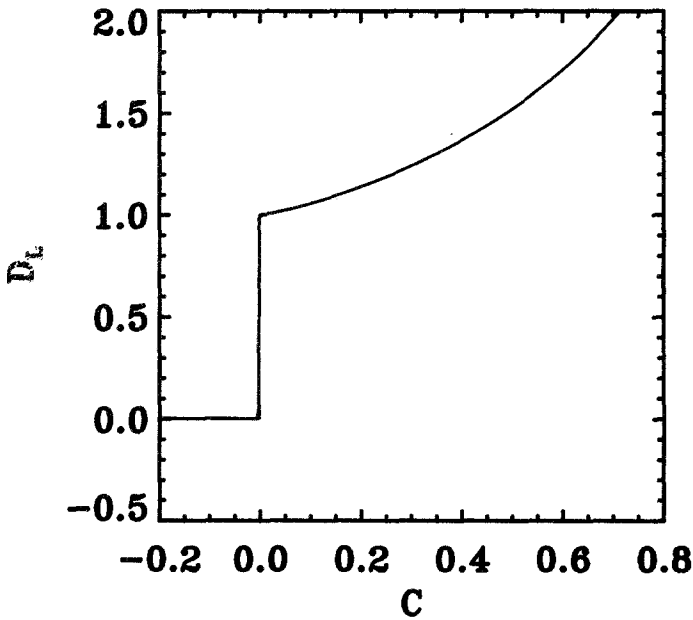

Fig. 13. The Lyapunov dimension D_L vs. the parameter C for the toral map.

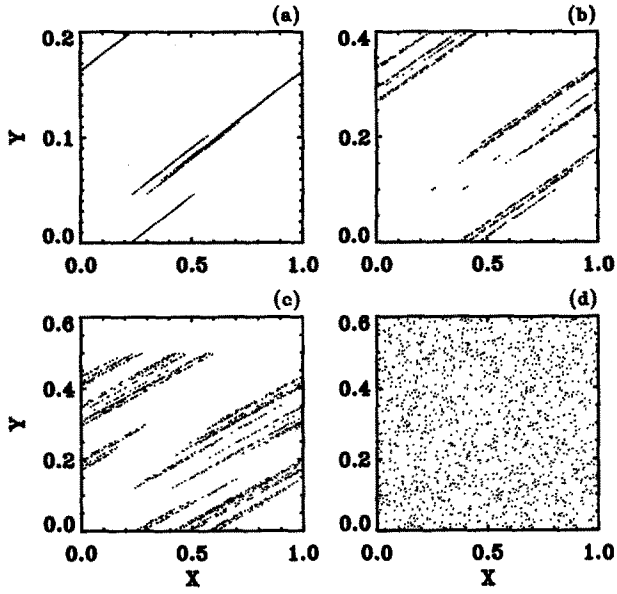

Fig. 14. The chaotic attractors of the toral map: (a) $C = 1/5$, (b) $C = 2/5$, (c) $C = 1/2$, and (d) $C = 1/B = 5/7$.

noteworthy that the nonuniformity of the attractor along the unstable manifold has little effect on the dimensions D_q.

6. THE STRUCTURE OF THE ATTRACTOR IN THE THREE-DIMENSIONAL TORAL MAP

In higher dimensions we encounter the possibility of high-dimension fractal attractors. Unlike the two-dimensional hyperbolic case, we do not have any general mathematical theorems to help us obtain the fractal structure of these chaotic attractors. However, in certain simple three-dimensional mappings we can obtain the fractal structure. Unfortunately the explicit characterization of these attractors is not simple. We will now consider some of the problems which arise when we try to characterize fractal structures in three or higher dimensions. We show that the Lyapunov dimension is unreliable as a gauge of the evolution of structure in strange attractors, in particular, how the negative Lyapunov exponents can produce dramatic effects on the structure of the attractor with no apparent change in its Lyapunov (Kaplan–Yorke) dimension D_L. Consider the

hyperbolic toral map L_B: $S \to S$,

$$B = \begin{pmatrix} a & b & c \\ d & e & f \\ g & h & i \end{pmatrix} \tag{34}$$

where the parameters of this matrix are $\in \mathbb{R}$. The ability to locate the unstable manifold is an important property that we will use in this section. Let us examine the possible structures that exist in $\mathbb{R}^3$.

The Lyapunov exponents are taken as follows: $\lambda_1 > 0 > \lambda_2 \geq \lambda_3$. For the particular case $\lambda_2 = \lambda_3$ the Lyapunov dimension D_L is $D_L = 1 - \lambda_1/\lambda_2$; by varying the magnitude of λ_2 in the range $(-\infty, -\lambda_1/2)$ the dimension D_L changes from 1 to 3. The different structures will be examined for this range of dimension. The eigenvalues of the matrix B will be chosen together with six of the parameters. The other three will be obtained by solving three simultaneous equations. The six parameters are $b = 1$, $c = 1/4$, $e = 0$, $f = 1/5$, $g = 0$, $h = 1$.

In this example the third Lyaponov exponent has no bearing on the Lyapunov dimension of the system. The fractal structure of the attractor is determined by the eigenvalues which are less than one. If the eigenvalues are of opposite sign and equal magnitude, we obtain a 2D Cantor set. In general it is the sign of the eigenvalues and their relative magnitude that determines the observed structure of the attractor. If we choose the eigenvalues to be $\varepsilon_1 = 1.4$, $\varepsilon_2 = 0.7$, and $\varepsilon_3 = 0.7$, the corresponding Lyapunov exponents are $\lambda_i = \log|\varepsilon_i|$. The corresponding parameters which give these eigenvalues are $a = 1.8219$, $d = -0.478668$, and $i = -0.421904$. A projection of the attractor onto the Y–Z plane is shown in Fig. 15. No information about the fractal structure is discernible from this projection. The eigenvector associated with the eigenvalue $\varepsilon_1 = 1.4$ is $\{0.920924, -0.34166, -0.18753\}^T$, where $\{0.920924, -0.34166, -0.18753\}^T$ is the transpose of $\{0.920924, -0.34166, -0.18753\}$. By rotating this eigenvector parallel to the X axis, the attractor will then be viewed in the Y'–Z' plane. The following rotation matrix is used:

$$\begin{pmatrix} X' \\ Y' \\ Z' \end{pmatrix} = \begin{pmatrix} \cos\beta\cos\alpha & -\cos\beta\sin\alpha & -\sin\beta \\ \sin\alpha & \cos\alpha & 0 \\ \sin\beta\cos\alpha & \sin\beta\sin\alpha & \cos\beta \end{pmatrix} \begin{pmatrix} X \\ Y \\ Z \end{pmatrix} \tag{35}$$

The coordinates X', Y', and Z' denote the rotated frame. The angles of rotation are $\alpha = 0.355257$ and $\beta = 0.188647$. A projection of the attractor onto the Y'–Z' plane is shown in Fig. 16a. A magnification of the indicated region is shown in Fig. 16b. This attractor has a two-dimensional

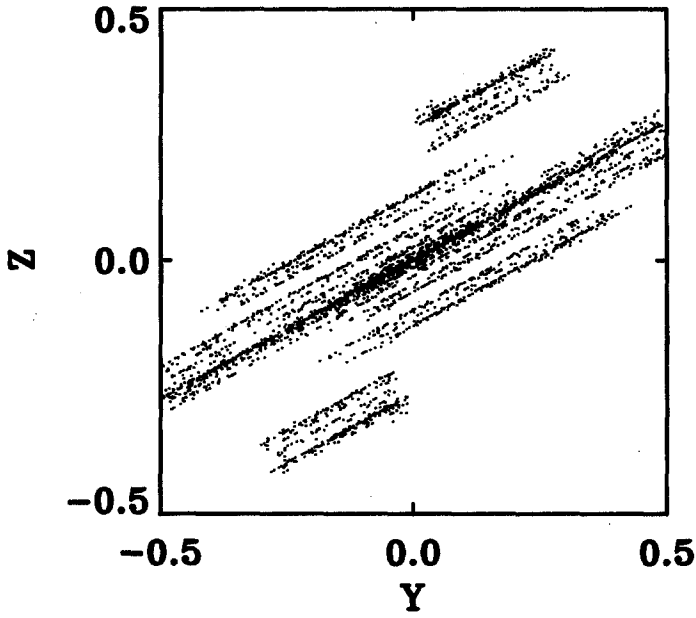

Fig. 15. A projection of a three-dimensional attractor onto the $Y-Z$ plane with parameters $a = 1.8219$, $d = -0.478668$, and $i = -0.421904$.

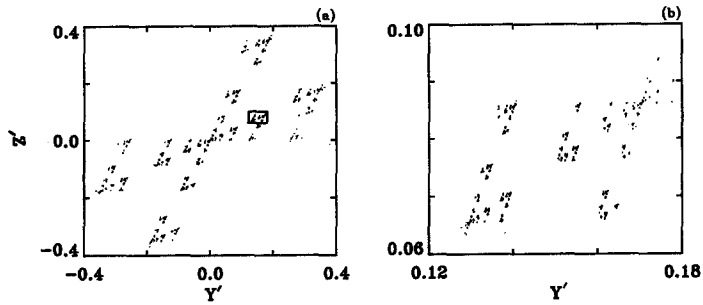

Fig. 16. The 3D toral map for the parameters $a = 1.8219$, $d = -0.478668$, and $i = -0.421904$. (a) The complete attractor. (b) Magnification of the indicated region. This suggests a two-dimensional Cantor set.

fractal structure with Lyapunov dimension $D_L = 1 - \log(1.4)/\log(0.7) = 1.94$. A calculation from the rotated time series Y' with 15,000 points gives $D_2 \approx 1.0$ for embedding dimensions of $d = 2-12$. The rotation of the system has reduced the dimension by 1.0, hence $D_2 \approx 2.0$, in agreement with the Lyapunov dimension. On the other hand, if we choose the

eigenvalues $\varepsilon_1 = 1.4$, $\varepsilon_2 = 0.8$, and $\varepsilon_3 = -0.8$, which gives the parameters $a = 1.95$, $d = -0.6325$, and $i = -0.55$, the Lyapunov dimension is $D_L = 2.51$. Again the attractor is rotated to reveal the two-dimensional Cantor set. The phase space attractor is shown in Fig. 17a with a magnification shown in Fig. 17b.

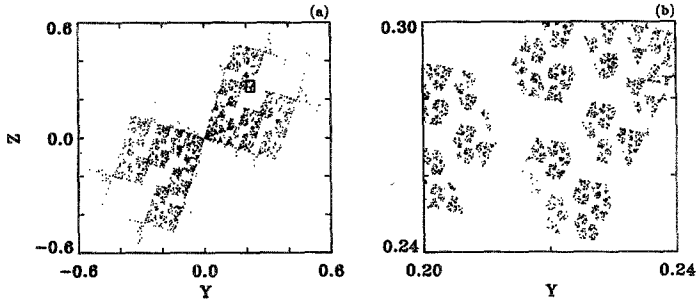

Fig. 17. The 3D toral map at $a = 1.95$, $d = -0.632568$, and $i = -0.55$. (a) The complete attractor. (b) A magnification of the indicated region.

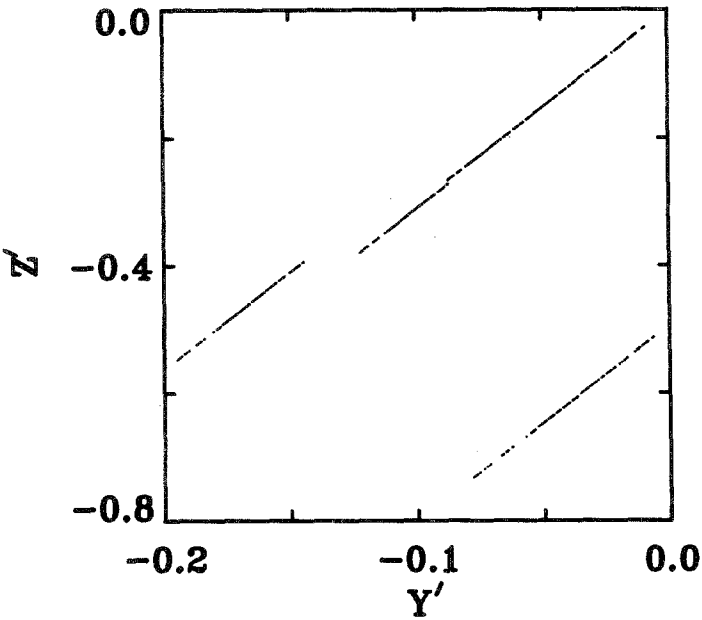

Fig. 18. The 3D toral map at $a = 0.724711$, $d = -0.0457843$, and $i = 1.275295$. Due to the nature of the Lyapunov exponents, points are repelled along the curves and attract transversely to the curves.

The two-dimensional fractals shown here were obtained from an optimum choice of Lyapunov exponents. In the majority of dynamical systems there is little control over the magnitude of the Lyapunov exponents. When $\lambda_3 < \lambda_2 < 0 < \lambda_1$ and when λ_3 is chosen to be a factor of six greater than λ_2, the two-dimensional fractal structure is not apparent. These problems can be further illustrated by selecting $\varepsilon_1 = 1.4$, $\varepsilon_2 = 0.7$, and $\varepsilon_3 = -0.1$, which gives $a = 0.724711$, $d = -0.0457843$, and $i = 1.27529$. Now the eigenvector associated with $\varepsilon_1 = 1.4$ is $\{-0.742696, -0.16692, -1.33863\}^T$. The system is rotated through the angles $\alpha = -0.221075$ and $\beta = -1.05369$. The attractor in the $Y'-Z'$ plane is shown in Fig. 18. This attractor appears to be one-dimensional; successive magnifications do not reveal a two-dimensional structure. The Lyapunov dimension is again $D_L = 1.94$ and the correlation dimension $D_2 \approx 1.0$ is obtained from the time series Y'. These two examples illustrate how a negative Lyapunov exponent can produce dramatic effects on the structure of the attractor with no apparent change to its Lyapunov dimension.

7. CONCLUSIONS

In this paper we have examined in detail the formation and evolution of fractal structure in the chaotic attractors of low-dimensional dynamical systems. In Section 2 we examined chaos in detail for the one-dimensional circle map. Using periodic enumeration techniques, we obtained the orbit structure of the map's attractor. The full spectrum of generalized dimensions D_q and the $f(\alpha)$ spectrum were also evaluated. For one-dimensional mappings the attractor is the closure of the unstable manifold. In Section 3 we examined Cantor sets in detail from the point of view of their $f(\alpha)$ spectra and their Lipschitz–Hölder scaling indices. These Cantor sets are fundamental to the understanding of chaos in one-, two-, and higher-dimensional systems. In Sections 4 and 5 the formation and evolution of fractal structure in two-dimensional systems was studied in detail using periodic orbit enumeration, generalized dimensional, and $f(\alpha)$ techniques. The Cantor structure was explicitly obtained in a number of cases. In particular, in Section 4, using $f(\alpha)$ techniques, we found that the local structure in the hyperbolic baker's attractor is the product of a line and a Cantor set and the Cantor set was exhibited explicitly. It was established that the increase in the Hausdorff dimension D_0 is due to changes in the dimension of the Cantor set. Using a modified version of the baker's map which has a pruned Cantor set, we obtained the $f(\alpha)$ spectrum for a range of dynamical parameters. In this particular case the pruning clipped the wings of the $f(\alpha)$ spectrum. We have found that the $f(\alpha)$ spectrum of a pruned Cantor set can be efficiently computed once the unstable periodic

orbits are obtained. The two- and three-dimensional nonuniform hyperbolic toral maps have relatively complex dynamics and insight into the nature of their unstable manifolds has allowed us to determine the nature of the underlining Cantor sets. These were studied in Sections 5 and 6. In three dimensions these Cantor sets can have both a one-dimensional and a two-dimensional structure. The problems in higher-dimension dynamical systems associated with high-dimension fractal attractors were also examined and some of the difficulties with the explicit characterization of these attractors were addressed. It was shown how a negative Lyapunov exponent can produce dramatic effects on the structure of the attractor with no apparent change to its Lyapunov dimension.

ACKNOWLEDGMENTS

This work is supported by EOLAS, the Irish funding agency for Science and Technology. We wish to thank Mark Daly for his invaluable help in preparing the figures and proofreading the manuscript.

REFERENCES

Aref, H., and Siggia, E. (1981). *Journal of Fluid Mechanics*, **109**, 435.
Arnold, V., and Avez, A. (1968). *Ergodic Problems of Classical Mechanics*, Benjamin, New York.
Auerbach, D., Cvitanovic, P., Eckmann, J., Gunaratne, G., and Procaccia, I. (1987). *Physical Review Letters*, **58**, 2387.
Auerbach, D., O'Shaughnessy, B., and Procaccia, I. (1988). *Physical Review A*, **37**, 2234.
Balatoni, J., and Renji, A. (1956). *Publications Mathematical Institute Hungarian Academy of Sciences*, **1**, 9.
Balazs, N., and Voros, A. (1989). *Annals of Physics*, **190**, 1.
Cvitanovic, P., Gunaratne, G., and Procaccia, I. (1988). *Physical Review A*, **38**, 1503.
De Arcangelis, L., Redner, S., and Coniglio, A. (1985). *Physical Review B*, **31**, 4725.
Devaney, R. (1989). *An Introduction to Chaotic Dynamical Systems*, 2nd ed., Addison-Wesley, Redwood, California.
Duong-van, M. (1987). *Nuclear Physics B (Proceedings Supplement)*, **2**, 521.
Eckmann, J. P., and Procaccia, I. (1986). *Physical Review A*, **34**, 659.
Eckmann, J. P., and Ruelle, D. (1985). *Review of Modern Physics*, **57**, 617.
Feigenbaum, M., Jensen, M., and Procaccia, I. (1986). *Physical Review Letters*, **56**, 1503.
Feigenbaum, M., Procaccia, I., and Tél, T. (1989). *Physical Review A*, **39**, 5359.
Graham, R., and Hamm, A. (1991). *Physical Review Letters*, **66**, 3089.
Grassberger, P., and Procaccia, I. (1983). *Physical Review Letters*, **50**, 346.
Grebogi, C., Ott, E., and Yorke, J. A. (1988). *Physical Review A*, **37**, 1711.
Gunaratne, G., and Procaccia, I. (1987). *Physical Review Letters*, **59**, 1377.
Halsey, T., Jensen, M., Kadanoff, L. P., Procaccia, I., and Shraiman, B. (1986). *Physical Review A*, **33**, 1141.
Hentschel, H., and Procaccia, I. (1983). *Physica*, **8D**, 435.
Isola, S. (1990). *Europhysics Letters*, **11**, 523.

Mandelbrot, B. (1977). *Annals of the Israeli Physical Society*, **1977**, 225.
Meakin, P., Stanley, H., Coniglio, A., and Witten, T. (1985). *Physical Review A*, **32**, 3364.
Procaccia, I. (1984). *Journal of Statistical Physics*, **36**, 649.
Procaccia, I. (1987). *Nuclear Physics B (Proceedings Supplement)*, **2**, 527.
Schroeder, M. (1991). *Fractals, Chaos and Power Laws*, Freeman, New York.
Schuster, H. (1988). *Deterministic Chaos*, VCH, Weinheim.
Stanley, H., and Meakin, P. (1988). *Nature*, **335**, 405.
Stauffer, D. (1985). *Introduction to Probability Theory*, Taylor & Francis, London.
Tél, T. (1988). *Zeitschrift für Naturforschung*, **43a**, 1154.
Vivaldi, F. (1987). *Proceedings of the Royal Society of London A*, **314**, 97.
Wiggins, S. (1988). *Global Bifurcations and Chaos*, Springer-Verlag, New York.
Wilson, K. G. (1979) *Scientific American*, **241**(2), 158.
Witten, Jr., A. T., and Sander, L. (1981). *Physical Review Letters*, **47**, 1400.